BMC Genomics

RESEARCH Open Access

Histone H3 K4 trimethylation occurs mainly at the origins of polycistronic transcription in the genome of *Leishmania infantum* promastigotes and intracellular amastigotes

Aurora Diotallevi[1†], Stefano Amatori[1†], Giuseppe Persico[2,3], Gloria Buffi[1], Enrica Sordini[1], Marco Giorgio[2,3], Mirco Fanelli[1†] and Luca Galluzzi[1*†]

Abstract

Background Trypanosomatids include the genera *Trypanosoma* and *Leishmania*, which are the etiological agents of important human diseases. These pathogens present unique mechanisms of gene expression characterized by functionally unrelated genes positioned in tandem and organized into polycistronic transcription units transcribed in a large pre-mRNA by RNA Polymerase II. Since most of the genome is constitutively transcribed, gene expression is primarily controlled by post-transcriptional processes. As in other organisms, histones in trypanosomatids contain a considerable number of post-translational modifications, highly conserved across evolution, such as the acetylation and methylation of some lysines on histone H3 and H4. These modifications have been mainly studied in *Trypanosoma* spp. The aim of this work was to elucidate the distribution of histone H3 lysine 4 trimethylation (H3K4me3) over the chromatin landscape of *Leishmania infantum*, the causative agent of canine and human leishmaniasis in the Mediterranean region. To this end, we investigated by chromatin immunoprecipitation (ChIP)-sequencing either the promastigotes (the flagellated motile form) and the amastigotes (the intracellular form) in an in vitro infection model.

Results The chromatin was prepared from THP-1 cells non infected, THP-1 cells infected with *L. infantum* MHOM/FR/78/LEM75, and THP-1 cells non infected and mixed with *L. infantum* MHOM/FR/78/LEM75 promastigotes. ChIP was conducted using anti-H3K4me3 or anti-H3K27me3 antibodies and ChIP-seq was performed on an Ion S5 sequencer. We showed that histone H3K4me3 is mainly enriched at transcription start sites (67%) or internally within the polycistronic transcription units (30%), with no differences between *L. infantum* promastigotes and amastigotes. Moreover, the enriched regions co-localize with another hallmark of transcriptional activation (histone H3 acetylation) in *L. major*, a species characterized by a high degree of synteny with *L. infantum*.

[†]Aurora Diotallevi and Stefano Amatori contributed equally to this work.

Mirco Fanelli and Luca Galluzzi contributed equally to this work.

*Correspondence:
Luca Galluzzi
luca.galluzzi@uniurb.it

Full list of author information is available at the end of the article

© The Author(s) 2025. **Open Access** This article is licensed under a Creative Commons Attribution-NonCommercial-NoDerivatives 4.0 International License, which permits any non-commercial use, sharing, distribution and reproduction in any medium or format, as long as you give appropriate credit to the original author(s) and the source, provide a link to the Creative Commons licence, and indicate if you modified the licensed material. You do not have permission under this licence to share adapted material derived from this article or parts of it. The images or other third party material in this article are included in the article's Creative Commons licence, unless indicated otherwise in a credit line to the material. If material is not included in the article's Creative Commons licence and your intended use is not permitted by statutory regulation or exceeds the permitted use, you will need to obtain permission directly from the copyright holder. To view a copy of this licence, visit http://creativecommons.org/licenses/by-nc-nd/4.0/.

Conclusions These findings expand our knowledge of the epigenomics of *Leishmania* parasites, focusing on epigenetic markers associated with transcription in *L. infantum*, and will contribute to elucidate the transcriptional mechanisms in these pathogens.

Keywords Amastigote, Epigenomics, H3K4me3, *Leishmania infantum*, Promastigote

Background

The family Trypanosomatidae includes two dimorphic genera, *Trypanosoma* and *Leishmania*, that cause important human diseases. *Trypanosoma cruzi* and *Trypanosoma brucei* are the etiological agent of American trypanosomiasis (Chagas disease) and African trypanosomiasis (sleeping sickness), respectively. The protozoan parasite *Leishmania* is the etiological agent of leishmaniasis, which occurs in three main forms: visceral (VL), cutaneous (CL) and mucocutaneous (MCL), depending on the *Leishmania* species and host characteristics [1]. About 20 *Leishmania* species are responsible for the infection in humans; among them, *Leishmania infantum* (syn. *L. chagasi*) is distributed in Mediterranean basin, West and Central Asia, and South America [2, 3]. *Leishmania* parasites are transmitted to their host by sand flies as metacyclic promastigotes. Once in the host, the parasites are ingested by macrophages where they differentiate into amastigotes, the parasitic form responsible for the maintenance and spreading of infection.

Trypanosomatids present unique mechanisms of gene expression: functionally unrelated genes are positioned in tandem and are organized into polycistronic transcription units (PTUs) transcribed in a large pre-mRNA by RNA Pol II. This pre-mRNA is processed into individual mature transcripts by trans-splicing, a process that adds a capped spliced leader (SL) RNA to the 5' end of each mRNA, and polyadenylation [4, 5]. The regions flanking the PTUs are defined Strand Switch Regions (SSRs). The RNA Pol II transcription initiates at divergent SSRs and terminates at convergent SSRs [5]. Transcription start sites (TSS) do not contain typical RNA Pol II core promoter element (e.g. TATA box) and post-transcriptional processes primarily control gene expression since most of the genome is constitutively transcribed [6].

Core histones H2A, H2B, H3, and H4 are highly conserved globular proteins with an N-terminal tail protruding from the central fold. In eukaryotes, two copies of each core histone, together with DNA wrapped around them, form the nucleosome, the basic unit of chromatin. The regulation of chromatin function is mainly based on histone post-translational modifications (PTMs), which consist of enzyme-mediated chemical modifications of specific histone residues, particularly at the N-terminal tail, and represent one of the most known epigenetic modifications. These modifications, combined with the activity of different ATP-dependent chromatin remodelers, control the chromatin state and play a major role in regulating gene expression, making chromatin accessible or not to transcriptional regulatory complexes [7]. The genes encoding histones H1, H2A, H2B, H3 and H4 are present also in trypanosomatids despite their sequences are quite divergent from those found in other organisms [8]. Moreover, histone variants (i.e., H2A.Z, H2B.V, H3.V and H4.V) have been identified in trypanosomatids, as also reported in higher organisms including humans [9]. Notably, the variants H3.V and H4.V, which seem to be unique to trypanosomatids, are not essential for their viability [10] and the variant H4.V has not been identified in *L. infantum*.

Chromatin organization in trypanosomatids has been mainly studied in *Trypanosoma* spp: in *T. brucei*, nucleosomes located in the proximity of TSS contain histone H2A.Z, H2B.V, H3, H4 and bromodomain factor 3 protein (BDF3). At the same time, transcription termination regions show enrichment of histone variants H3.V and H4.V [11]. Moreover, transcription termination sites (TTS) often contain an active pol III transcribed tRNA gene [12]. Regarding histone PTMs, high-resolution mass spectrometry studies identified over 150 modifications in both *T. cruzi* [13, 14] and *T. brucei* [15, 16], many of them showing global fluctuations during the life cycle [17]. As observed in higher eukaryotes, specific histone PTMs have been linked to genomic functional regions. This is the case of histone H4 lysine 10 acetylation (H4K10ac) and histone H3 lysine 4 trimethylation (H3K4me3) that were found to be enriched at the TSS in *T. brucei* [11, 18]. In addition, histone H3 lysine 76 methylation (H3K76me) was found to regulate DNA replication in *T. brucei*, showing a behavior similar to that of mammal histone H3 lysine 79 methylation (H3K79me) [19, 20].

On the other hand, histone modifications landscape has been poorly investigated in *Leishmania* species. The acetylation at lysines 9/14 of histone H3 has been demonstrated in TSS regions in *L. major* [21], while acetylation of lysines 4/10/14 on histone H4 (H4K4ac, H4K10ac, H4K14ac) have been described in *L. donovani* [22–24]. Recently, a comprehensive work elucidated the distribution of histone variants and PTMs over the chromatin landscape of *L. tarentolae*, a non-pathogenic species belonging to subgenus Sauroleishmania [25], evidencing the enrichment of H3K4me3 at the TSS as observed in *T. brucei*. Nevertheless, histone PTMs have never been investigated in *L. infantum* genome, even more in the context of cellular infection. In this work, using chromatin immunoprecipitation (ChIP) and massive parallel

DNA sequencing, we provide evidence that H3K4me3 occurs in *L. infantum* genome, and we show that TSS of polycistronic transcription units are enriched by this modification in both promastigotes and intracellular amastigotes.

Methods

Leishmania infantum culture

Leishmania infantum strain MHOM/FR/78/LEM75 was provided by the World Organization for Animal Health (OIE) Reference Laboratory National Reference Center for Leishmaniasis (C.Re.Na.L.) located in Palermo (Italy). The parasites were cultivated at 26 °C in Evans' Modified Tobie's Medium (EMTM) [26]. Every 5 days stationary promastigotes were transferred to fresh medium (ratio 1:5). To obtain axenic amastigotes, 1×10^7 promastigotes/ml were differentiated in a specific medium, consisting of M199 medium supplemented with 25% FBS, 1% penicillin/streptomycin, and 10 mM succinic acid. The medium was titrated to pH 5.5 with HCl and filtered to sterilize, and the suspension was incubated at 37 °C in a 5% CO_2 incubator. After 24 h, the culture was diluted 1:10 with the amastigote medium described above, and the incubation was prolonged for an additional 4 days.

Cell culture-derived macrophages and infection

The human monocytic cell line THP-1 (ECACC 88081201) was cultured in RPMI-1640 medium supplemented with 10% heat inactivated Fetal Bovine Serum (FBS), 2 mM L-glutamine, 1% penicillin/streptomycin at 37 °C and 5% CO_2. To differentiate monocytes into macrophage-like cells, 1.5×10^6 cells were stimulated with 10 ng/ml phorbol myristic acid (PMA) for 72 h in 60 mm dishes. *L. infantum* MHOM/FR/78/LEM75 stationary promastigotes were used to infect THP-1-derived macrophages with a parasite-to-cell ratio of 10:1 as described [27]. To synchronize the entrance of parasites into cells, dishes were centrifuged at 450 x g for 3 min. Infection was repeated twice. After 24 h, the medium was changed to remove free parasites. Then, after 48 h from infection (to allow amastigotes differentiation), cells were fixed by adding the cross-linking solution (50 mM Hepes pH 7.5, 11% Formaldehyde, 1 mM Na_2EDTA, and 0.1 M NaCl) in a volume equivalent to 1/10 of the culture medium as described in the paragraph "Chromatin preparation" and harvested by scraping.

The infection index was calculated in a separate dish containing cells stained with Hoechst dye, by multiplying the percentage of infected macrophages by the average number of amastigotes per cell. At least 200 total macrophages were counted for each infection.

Table 1 Sample description

Description	Immunoprecipitation	Sample ID
THP-1 cells non-infected	H3K4me3	27
THP-1 cells non-infected	H3K27me3	28
THP-1 cells infected (infection index = 463 ± 36)[a]	H3K4me3	26
THP-1 cells infected (infection index = 463 ± 36)[a]	H3K27me3	32
THP-1 cells spiked with promastigotes[b]	H3K4me3	17

[a]THP-1 cells infected for 48 h with *L. infantum* MHOM/FR/78/LEM75

[b]THP-1 cells non infected and mixed with a number of *L. infantum* MHOM/FR/78/LEM75 promastigotes comparable to the number present in infected cells

Chromatin preparation

Chromatin was prepared starting from infected THP-1 cells to allow the study of amastigotes chromatin directly in the intracellular context, exploiting the THP-1 chromatin as heterologous "carrier" chromatin, as previously reported for different applications [28]. In details, chromatin was prepared from the samples listed in Table 1: (i) THP-1 cells non infected (two petri dishes pooled together, 3×10^6 cells); (ii) THP-1 cells infected for 48 h with *L. infantum* MHOM/FR/78/LEM75 (two petri dishes pooled together, 3×10^6 cells). (iii) THP-1 cells non infected and mixed with a number of *L. infantum* MHOM/FR/78/LEM75 promastigotes comparable to the number present in infected cells (two petri dishes pooled together, 3×10^6 cells and 24×10^6*L. infantum* promastigotes). This last sample allowed chromatin preparation from *L. infantum* promastigotes using the THP-1 chromatin as carrier, assuring the same experimental conditions used for intracellular amastigotes in infected cells. All THP-1 cells were differentiated into macrophage-like cells by PMA treatment before chromatin preparation.

Cells were cross-linked for 10 min at 37 °C by adding the cross-linking solution (50 mM Hepes pH 7.5, 11% Formaldehyde, 1 mM Na_2EDTA, and 0.1 M NaCl) in a volume equivalent to 1/10 of the culture medium. The cross-linking reaction was stopped by addition of glycine at a final concentration of 0.125 M. Cells were then washed twice with ice-cold PBS and finally resuspended in 0.5 ml of lysis buffer (10 mM Tris-HCl pH 7.4, 0.15 M NaCl, 3 mM $CaCl_2$, 2 mM $MgCl_2$, 0.5% Tween20, 1 mM PMSF, and 10 µg/mL RNase A) and incubated 30 min at room temperature on a rotating platform. When not specified, all centrifugations were performed at 17,860×g for 3 min at + 4 °C. After resuspension in 0.3 ml of extraction buffer (10 mM Tris-HCl pH 7.4, 0.15 M NaCl, 3 mM $CaCl_2$, 2 mM $MgCl_2$, 0.1% SDS), samples were sonicated with three pulses of 30 s each with an amplitude of 40% (using a – 20 °C refrigerated thermoblock), interrupted by 60 s pauses, using the EpiShear sonicator (Active Motif, Carlsbad, CA, USA) as already described [29]. After being cleared by centrifugation, at 9,500×g for 5 min at

room temperature, supernatants containing chromatin were saved, and an aliquot of 30 µl was purified using the PCR Purification Kit (QIAGEN, Hilden, Germany). The DNA amount was estimated by Qubit (Invitrogen, Eugene, OR, USA) using the dsDNA HS Assay Kit (Invitrogen, Eugene, OR, USA) and chromatin size was checked by agarose gel electrophoresis.

Chromatin immunoprecipitation (ChIP) and sequencing

The chromatin immunoselection was conducted as previously described [30, 31] using anti-H3K4me3 (#39159, Lot. 2219006; Active Motif, Carlsbad, CA, USA) or anti-H3K27me3 (#07-449, Lot. 3091919; Millipore, Temecula, CA, USA) antibodies. *Leishmania* H3K4me3 was studied using an anti-human H3K4me3 polyclonal antibody because of the histone H3 N-terminal sequence conservation across all eukaryotes, including trypanosomatids (Fig. 1). Multiple sequence alignment of histone H3 from *H. sapiens*, *M. musculus*, *S. cerevisiae*, *L. infantum*, *L. major*, *L. braziliensis*, *T. brucei* and *T. cruzi* was performed by MUSCLE (MUltiple Sequence Comparison by Log-Expectation) (www.ebi.ac.uk) with CLUSTALW output format parameters. Among the first 8 residues, 5 are identical and the remaining three show strong similar properties with human sequences. This finding supported the use of anti-H3K4me3 antibody to immunoprecipitate *L. infantum* chromatin. It is noteworthy that the same antibody batch has proven to be specific for H3K4me3 in previous works conducted on human samples [32–34]. The anti-human H3K27me3 antibody was used as negative control for *L. infantum* chromatin immunoprecipitation since sequence surrounding K27 is scarcely conserved in trypanosomatids (Fig. 1). All IP samples analyzed in this study are listed in Table 1.

Immunoselected DNA, once purified and quantified, was preliminary used to test the immunoprecipitation specificity by qPCR; then, two ng were processed for libraries preparation using the Ion Plus Fragment Library Kit (Thermo Fisher Scientific), following manufacturer's instructions. Sequencing was performed on an Ion S5 sequencer (Thermo Fisher Scientific) with the Ion 540 chip.

Locus-specific analysis of immunoselected DNA

The immunoselected DNA obtained by ChIP was analyzed by real-time quantitative PCR (qPCR) to evaluate the specificity of the immunoprecipitation by amplifying two target sequences on THP-1 cells corresponding to the promoter region of VCL and HAPLN1 genes (known to show an opposite behavior in terms of H3K4me3 and H3K27me3 enrichment in human cells) [31]. Purified DNA was analyzed in triplicate by qPCR using the Fast Start SYBR Green Master Mix (Roche, Mannheim, Germany) and the Rotor-Gene 6000 thermocycler (Corbett Life Science, Sydney, Australia) as previously reported [29]. The primer pairs used for this analysis were VCL-F: 5′-ATGCCAGTGTTTCATACGCG-3′, VCL-R: 5′-CGCCCTCCTCGTGCATTAT-3′, HAPLN1-F: 5′-TCGGATGCTCTCAAGTTCTGC-3′, HAPLN1-R: 5′-TCGCCCAGAGACAAACTTAAGG-3′.

ChIP-Seq analysis

The ChIP-seq reads were filtered for PCR duplications and aligned to *L. infantum* JPCM5 genome (TriTrypDB-43_LinfantumJPCM5_Genome; equivalent to GenBank assembly GCA_900500625.2) by Torrent Suite Software 5.12.0. The BAM files were deposited in Sequence Read Archive (SRA) (BioProject ID: PRJNA1069007) with accession numbers

```
                    4                          27
H.sapiens           ARTKQTARKSTGGKAPRKQLATKAARKS---APATGGVKKPHR-YRPGTVALREIR
M.musculus          ARTKQTARKSTGGKAPRKQLATKAARKS---APATGGVKKPHR-YRPGTVALREIR
S.cerevisiae        ARTKQTARKSTGGKAPRKQLASKAARKS---APSTGGVKKPHR-YKPGTVALREIR
L.infantum          SRTKETAR-------AKRTITSKKSKKA---PSAASGVKKSHRRWRPGTCAIREIR
L.major             SRTKETAR-------AKRTITSKKSKKA---PSAVSGVKMSHRRWRPGTCAIREIR
L.braziliensis      SRTKETAR-------TKRSITAKKSKKA---PSAVSGLKKVHRRWRPGTCAIREIR
T.brucei            SRTKETAR-------TKKTITSKKSKKASKGSDAASGVKTAQRRWRPGTVALREIR
T.cruzi             SRSKETAR-------SKRTITSKKSKKAPKAPGAATGVKHAQRRWRPGTVALREIR
                    :*:*:***       ... :::* :.*:   . :. *:*  :* :.*** *:****
```

Fig. 1 CLUSTAL multiple sequence alignment by MUSCLE of N-terminal tail of histone H3. Alignment of N-terminal histone H3 sequences from *H. sapiens* (UniProt ID: P68431), *M. musculus* (UniProt ID: P68433), *S. cerevisiae* (UniProt ID: P61830), *L. infantum* (UniProt ID: A4HUJ9), *L. major* (UniProt ID: Q4QHB5), *L. braziliensis* (UniProt ID: A4H675), *T. brucei* (UniProt ID: Q4GYX7) and *T. cruzi* (UniProt ID: V5BEW0). The lysines 4 and 27 in human sequence are in bold underlined. (*) identities; (:) conservation between groups of strongly similar properties; (.) conservation between groups of weakly similar properties

SAMN39609176, SAMN39609177, SAMN39609178, SAMN39609179, SAMN39609180 for samples 27, 28, 26, 32, 17, respectively (Table 1). The BAM files were uploaded to the Galaxy web platform, and we used the public server at "usegalaxy.org" to analyze the data [35]. The BAM files were checked for similarity by principal component analysis using multiBamSummary and plotPCA tools. The BAM files were converted to BigWig for visualization in the JBrowse Genome Browser. Peak calling was performed using non-duplicate reads with MACS2 callpeak version 2.1.1.20160309, using ChIP-seq data from uninfected THP-1 cells or infected THP-1 immunoprecipitated with anti-H3K27me3 as controls. Parameters were used as follows: effective genome size = 3.2e+07; Build Model = nomodel; q-value cutoff for peak detection = 0.05; qvalue cutoff for broad regions = 1.00e-05.

Co-localization of H3K4me3 peaks in *L. infantum* and H3 acetylated peaks in *L. major*

The BAM file from sample 17 (i.e., THP-1 cells spiked with promastigotes and H3K4me3-immunoprecipitated) was processed with bedtools bamtofastq in order to retrieve.fastq file. Then, reads of fastq file were mapped on *L. major* strain Friedlin genome (downloaded from https://tritrypdb.org/tritrypdb/app/downloads) using bwa mem. All unmapped reads were removed using samtools while PCR duplicated were removed using markdup -r function of samtools. Peak calling was done on mapped reads using macs callpeak with the following parameters: effective genome size = 3.3e+07; Build Model = nomodel; q-value cutoff for peak detection = 0.05; qvalue cutoff for broad regions = 1.00e-05. The enriched identified regions were intersected using bedtools with the 188 peaks of acetylated H3 histone as identified by Thomas et al. [21], in order to find co-localized regions. Tracks were visualized on JBrowse to manually check the results. An additional comparison was also performed between *L. infantum* H3K4me3 peaks (represented in Additional file 1_Table S1) and the 188 peaks of acetylated H3 histone as identified by Thomas et al. [21].

Western blot analysis and coomassie staining

Western blotting analysis was performed as previously reported [31]. Briefly, proteins were subjected to SDS polyacrylamide gel electrophoresis under reducing conditions and transferred to nitrocellulose membranes (Cityva, Little Chalfont, Buckinghamshire, UK). Membranes were blocked with 5% (w/v) milk in TBS buffer and 0.5% (v/v) Tween 20 (TBST) for 45 min at room temperature, and then incubated for 2 h at room temperature with the following antibodies: anti-human H3K4me3 rabbit polyclonal antibody (Active Motif, Carlsbad, CA, USA – 1:1000 dilution in TBST with 5% milk) and anti-human histone H3 rabbit monoclonal antibody (Upstate Biotech, Lake Placid, NY, USA – 1:500 dilution in TBST with 5% milk). Antibody reactivity was monitored with horseradish peroxidase (HRP)-conjugated anti-rabbit IgG, using an enhanced chemiluminescence detection ECL kit (Cityva, Little Chalfont, Buckinghamshire, UK) and images were acquired using the Vü-C Imaging system (PopBio, Cambridge, UK).

Coomassie staining was performed using 0,1% CBB R-250 (BDH Biochemical, Umm Ramool, Dubai, UAE) dissolved in 50% methanol, 10% acetic acid and 40% dH_2O. The gel was stained for 1 h at room temperature and destained with 50% methanol, 10% acetic acid and 40% dH_2O.

Statistical analysis

The Spearman's correlation, linear regression analyses, ANOVA and t-test were performed using Graphpad Prism version 5.0.

Results

Validation of ChIP-seq data and general characterization of detected peaks

First, we checked the ability of the anti-H3K4me3 antibody to recognize this modification in *L. infantum* promastigotes and amastigotes. To this end, histone protein patterns of *L. infantum* and control human NB4 cells were analyzed by Coomassie staining of SDS-PAGE separated total cellular lysates. As shown in Fig. 2A, a band of 14.6 kDa, corresponding to *L. infantum* histone H3 (UniProt ID: P40285), has been identified, while histone proteins from human cells showed the canonic migration pattern allowing, even in this case, the identification of the band corresponding to human histone H3 (15.4 kDa). Western blotting analysis of total cellular lysates was performed using antibodies directed against histone H3 total protein and K4 trimethylation of histone H3 (H3K4me3) (Fig. 2B). The results indicated that the band detected by both antibodies overlap with the one identified as histone H3 by Coomassie staining in both *L. infantum* and human lysates.

Afterwards, histone H3 PTM distribution was studied in both *L. infantum* amastigotes and promastigotes. In the first case, we analyzed the epigenomic distribution of H3 PTM directly in intracellular amastigotes, preparing *L. infantum* chromatin together with the chromatin of infected THP-1 cells. This allowed to study the epigenetic marker of interest in physiological infection conditions. Contextually, to gain knowledge of potential differences between the amastigote and promastigote stages, we analyzed the H3 PTM in *L. infantum* promastigotes (the cultured motile form). To maintain the same experimental conditions, THP-1 cells were added just before chromatin preparation. Therefore, chromatin was

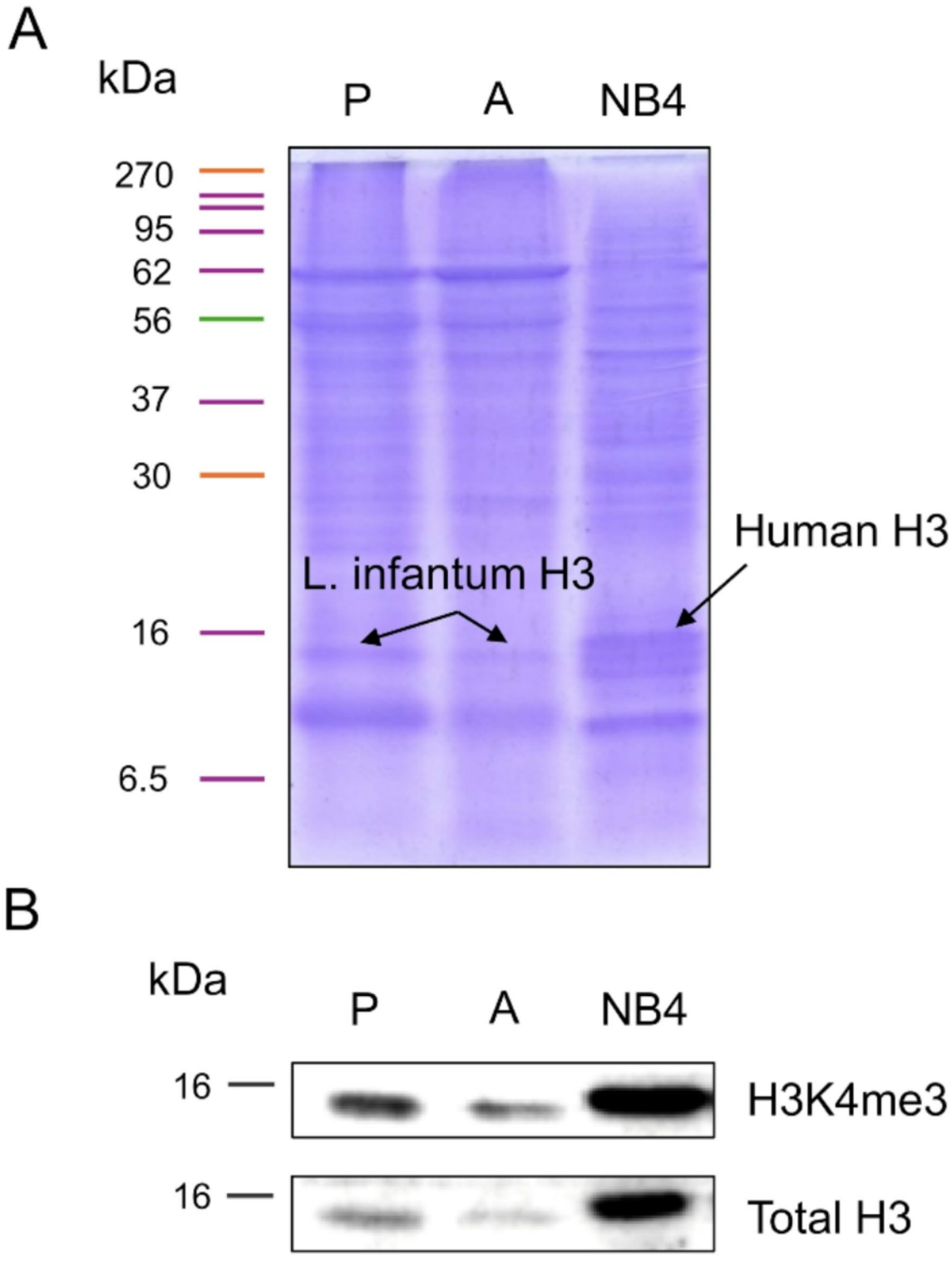

Fig. 2 Evaluation of the ability of the anti-H3K4me3 antibody used in the study to recognize its target in *L. infantum*. (**A**) Total lysates from *L. infantum* promastigotes (P), amastigotes (A) and human acute promyelocytic leukemia NB4 cell line were separated by SDS-PAGE and stained with Coomassie Brilliant Blue to observe histones separation pattern. Putative *Leishmania* histone H3 (~ 15 kDa) and human histone H3 (~ 16 kDa) are indicated by arrows. (**B**) Western blot analysis of whole-cell lysates of *L. infantum* promastigotes (P), amastigotes (A) and NB4 cell line performed with the anti-H3K4me3 antibody used in the study (upper line) and an anti-histone H3 antibody (lower line)

extracted from infected THP-1 cells, non-infected THP-1 cells and THP-1 cells spiked with *L. infantum* promastigotes (Table 1) and immunoprecipitated with antibodies directed against H3K4me3 and H3K27me3. Due to the poorly conserved sequence surrounding K27 in *Leishmania* histone H3 (Fig. 1), the anti-H3K27me3 antibody was intended as negative control of *Leishmania* chromatin immunoprecipitation. The resulting purified DNA was preliminary analyzed by qPCR to evaluate the specificity of the immunoselection; for this technical evaluation, we focused on selected THP-1 control regions by amplifying the promoter region of known THP-1 expressed or non-expressed genes, confirming the expected enrichments (Additional file 2).

ChIP-seq generated an average of 22 million ~ 150 bp single end reads from each immunoprecipitated sample. The summary of sequencing output statistics is described in Additional file 3_Table S2.

Reads aligned to *L. infantum* genome were analyzed by principal component analysis (PCA) revealing that negative control samples (i.e., samples immunoprecipitated with anti-H3K27me3 antibody and non-infected cells immunoprecipitated with anti-H3K4me3) clustered together, while they were distinct from the samples containing promastigotes or amastigotes immunoprecipitated with anti-H3K4me3 (Fig. 3). ChIP-seq reads of immunoprecipitated DNA obtained with anti-H3K27me3 showed only 6 small peaks in *L. infantum* genome, corresponding to telomeric sequences on chromosomes 7, 8, 9, 11, 12, 31, corroborating its use as negative control (Additional file 1_Table S1). Instead, anti-H3K4me3 ChIP-seq reads aligned with the *L. infantum* genome showed 135 major enriched DNA regions. A complete representation of enriched regions is provided in Additional file 4 and Additional file 1_Table S1. Most of the H3K4me3 peaks were located at the beginning of all polycistronic transcription units (at the divergent or telomeric transcription start sites) ($n = 90$; 67%), with two exceptions: a TSS in chromosome 15 (nucleotide 204,000) and a TSS in the telomeric region of Chromosome 22 (nucleotide 780,000), in which the H3K4me3 peaks were missing. Other H3K4me3 peaks were found internally within the PTU ($n = 40$; 30%). Among them, 12 were found in correspondence to tRNA or snoRNA genes, 12 were near centromeres, as inferred from *L. major* KKT1 Chip-seq [36], and the remaining were not associated with any apparent features. Further, four H3K4me3 peaks were found in telomeric regions at the end of PTU of chromosomes 1 (near centromere), 7, 12 and (to a lesser extent) 27. Finally, one broad peak was found in correspondence to a rRNA locus on chromosome 27. Representative examples are depicted in Fig. 4.

L. infantum promastigotes and amastigotes share the same H3K4me3 enriched regions

To investigate differences in the H3K4me3 pattern between promastigotes and intracellular amastigotes, ChIP-seq experiments were performed either using infected cells (containing amastigotes) or non-infected cells spiked with fixed *L. infantum* promastigotes. After peak calling, the number of H3K4me3 peaks was evaluated for samples containing amastigotes and promastigotes. We found a substantial agreement in H3K4me3 peak location between samples (Fig. 5 and Additional file 1_Table S1). Visual analysis of BigWig files allowed to identify the same 135 enriched regions in all samples (Fig. 5A). Moreover, these regions showed comparable widths in promastigotes and amastigotes (Fig. 5B).

H3K4me3 peaks in *L. infantum* co-localize with H3 acetylated peaks in *L. major*

There are few data in literature regarding *Leishmania* spp chromatin organization or histone modifications and no data are available for *L. infantum*. To gain insight the histone PTMs organization in *L. infantum* genome, we performed a comparative analysis between H3K4me3 peaks obtained in *L. infantum* and H3 acetylated peaks obtained by chip-on-chip analysis in the related species *L. major* [21], which shows a high degree of genome conservation in terms of both gene content and gene synteny [37]. The comparison -performed as described in methods- showed that about 90% *L. infantum* H3K4me3 peaks co-localized with *L. major* H3 acetylated peaks (169 out of 188), confirming the nucleosome positions along the genomes of these two species. All comparison results are summarized in Additional file 5_table S3 and visualized in Additional file 6. Very similar results were found performing the comparison between *L. infantum* H3K4me3 peaks and *L. major* H3 acetylated peaks aligned to their respective genomes (additional file 7_table S4). Excluding the repetitive regions at the beginning of chromosome 2 and at the end of chromosomes 7 and 25, several acetylated H3 peaks inside some PTU in chromosomes 13, 19, 23, 24, 26, 30, 34 and 35 of *L. major*, do not have counterpart H3K4me3 peaks in the orthologous regions of *L. infantum* (Fig. 6).

As already noticed by Thomas et al. for H3 acetylation in *L. major* [21], all *L. infantum* H3K4me3 peaks are associated with increased AT content (i.e., lower GC content). In fact, the average GC content along the 36 chromosomes is 60.4%±1.4% while the average GC content in H3K4me3 peak mapping regions appears significantly lower for all chromosomes (one-way ANOVA with Bonferroni post test; $p < 0.01$) ranging from 47.4%±2.7% (chr 19) to 55.3%±2.0 (chr 31) (Fig. 7).

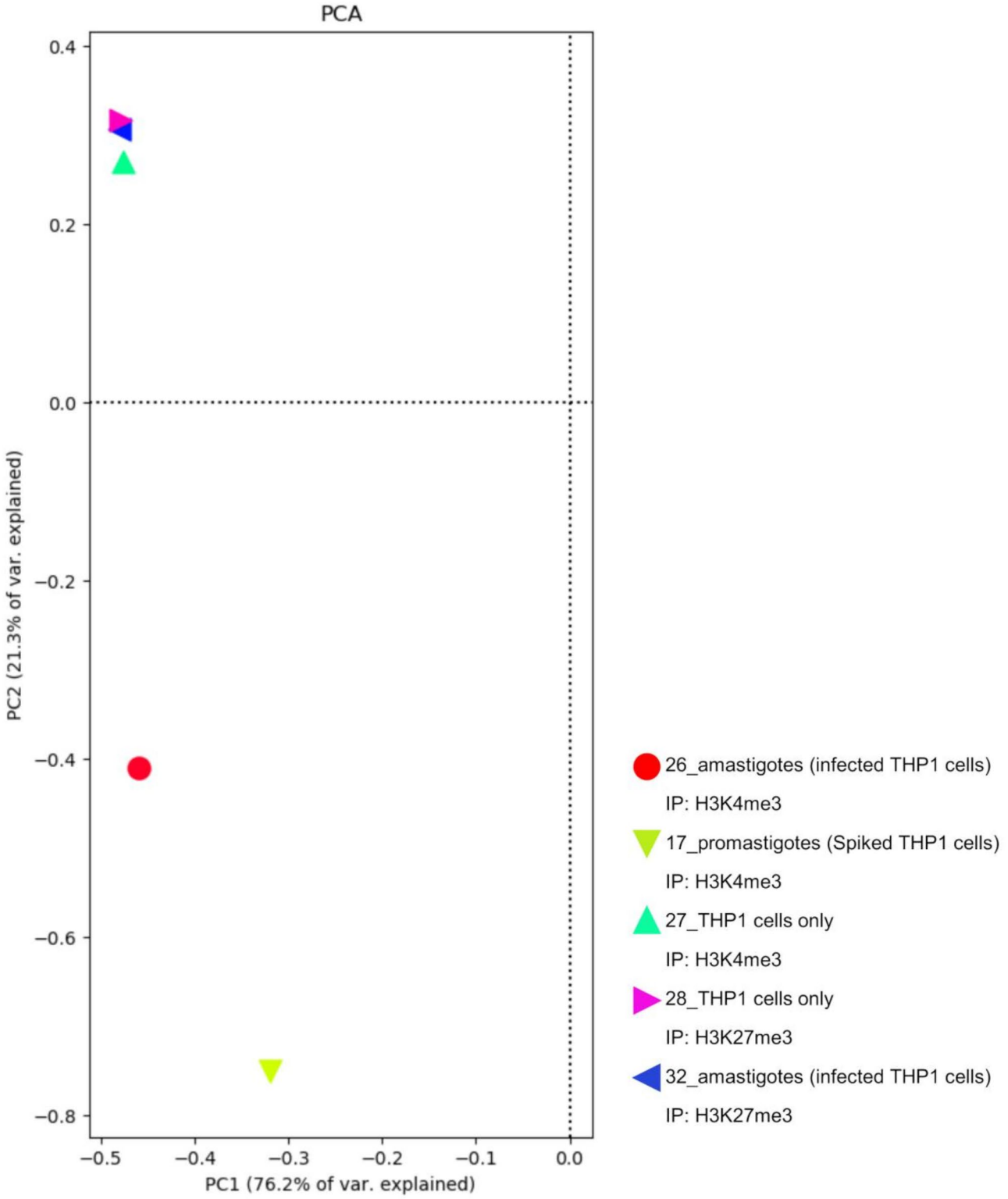

Fig. 3 Clustering of H3K4me3 and H3K27me3 ChIP-seq reads. Principal component analysis (PCA) plot with the corresponding percentages of variance (indicated in the x axis for PCA1 and on the y axis for PCA2) shows a separate clustering of samples immunoprecipitated with anti-H3K4me3 and containing *Leishmania* DNA (sample n. 17, 26) from the samples immunoprecipitated with anti-H3K27me3 or not containing *Leishmania* DNA (sample n. 27, 28, 32)

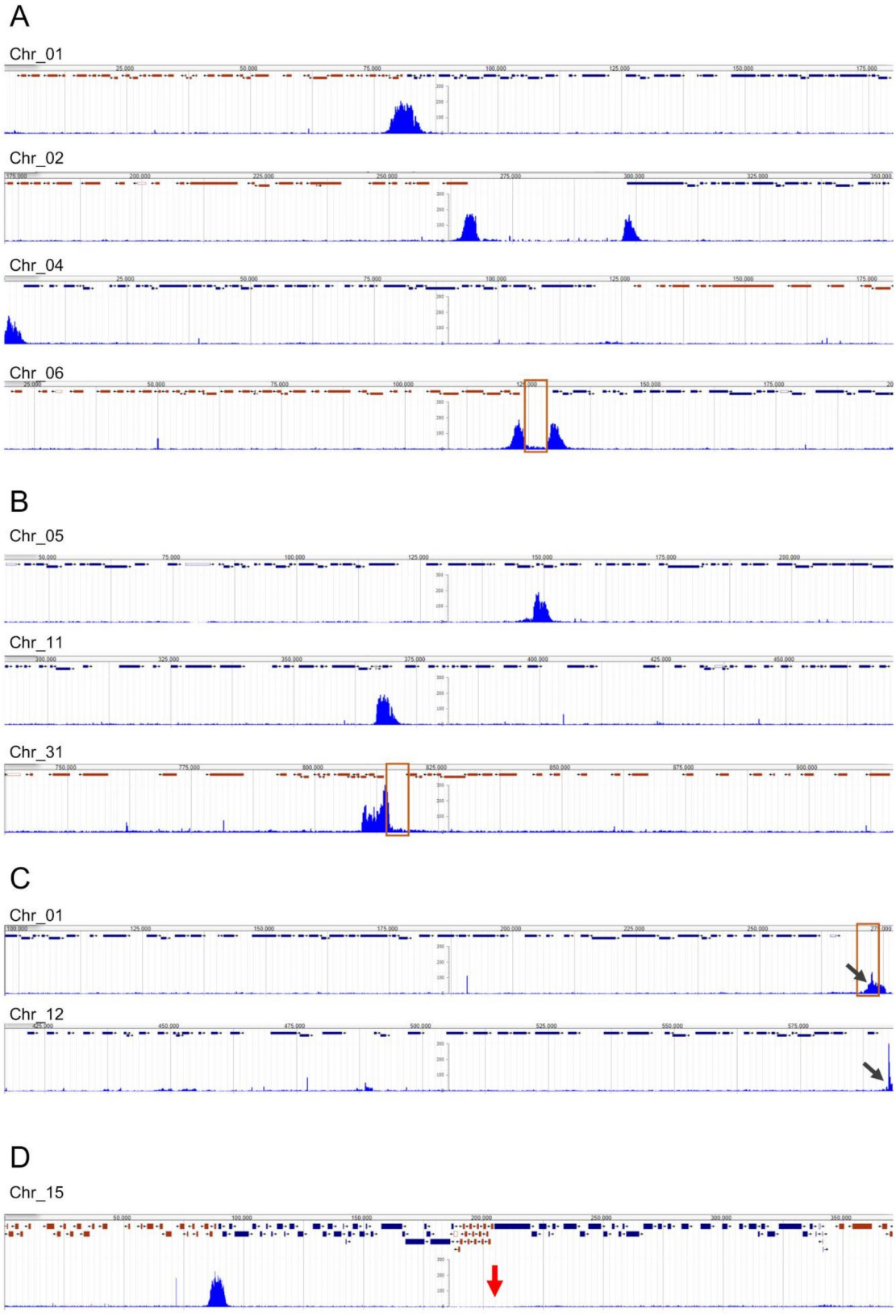

Fig. 4 (See legend on next page.)

(See figure on previous page.)

Fig. 4 Location of H3K4me3 enriched regions along *L. infantum* chromosomes. (**A**) Examples of H3K4me3 enriched regions at telomeric TSS (chromosome 4) and divergent TSS (chromosomes 1, 2, 6). The peaks in chromosome 2 are located 5′ and 3′ to splice leader RNA array (not annotated). (**B**) The H3K4me3 enriched regions were also found internally within PTU, in some case associated to tRNA genes (e.g., chromosome 11) or near centromeres (e.g., chromosome 31). (**C**) Examples of H3K4me3 enriched regions at telomeric regions at the end of PTU (chromosome 1 and 12). (**D**) missing H3K4me3 enriched region at TSS in chromosome 15 is indicated by a red arrow. Chromosome portions of about 180 kb are shown. Overlapping enriched regions were obtained for promastigotes and amastigotes but only tracks from promastigotes (sample ID 17) are visualized here. Boxed regions indicate putative centromeres, as inferred from *L. major* KKT1 Chip-seq (36)

Discussion

The histones in trypanosomatids carry several post-translational modifications, as observed in other organisms. Some of these modifications are conserved across evolution, such as the acetylation and methylation of some lysines on histone H4 and H3 [10, 18]. Most studies regarding chromatin organization in trypanosomatids have been performed in *Trypanosoma* spp., while studies on histone modifications landscape in *Leishmania* spp. are still limited. Recently, a study conducted on *L. tarentolae* confirmed that the distribution of histone variants in *Leishmania* is similar to that previously reported for *T. brucei* [25]. To further expand the study of histone PTMs in pathogenic *Leishmania* species, we explored for the first time histone H3K4me3 in *L. infantum*. ChIP was performed from amastigotes and promastigotes maintaining the same chromatin background from THP-1 cells. In fact, while ChIP from amastigotes was performed from infected THP-1 cells, ChIP from promastigotes was performed on parasites spiked with THP-1 cells immediately before chromatin preparation. The study of *L. infantum* chromatin in the context of infection allowed us to exclude biases related to non-physiological conditions (e.g., in vitro amastigote differentiation), also considering the crosstalk that is established between the pathogen and the host cell. For example, it is known that *Leishmania* histone H3 is released by the parasite and can be incorporated into host chromatin modulating its structure [38].

First, we confirmed that H3K4me3, which is typically associated with transcriptional activation in other eukaryotes, was found at the beginning of PTU of protein-coding genes transcribed by RNA Pol II, and upstream of RNA genes transcribed by RNA Pol I (rRNA) and RNA Pol III (snoRNA, tRNA). Moreover, H3K4me3 enriched regions were also found near centromeres, as observed in *L. tarentolae* [25].

Notably, we pointed out that H3K4me3 enriched regions correlate between promastigotes and amastigotes and that those regions have similar width. The average

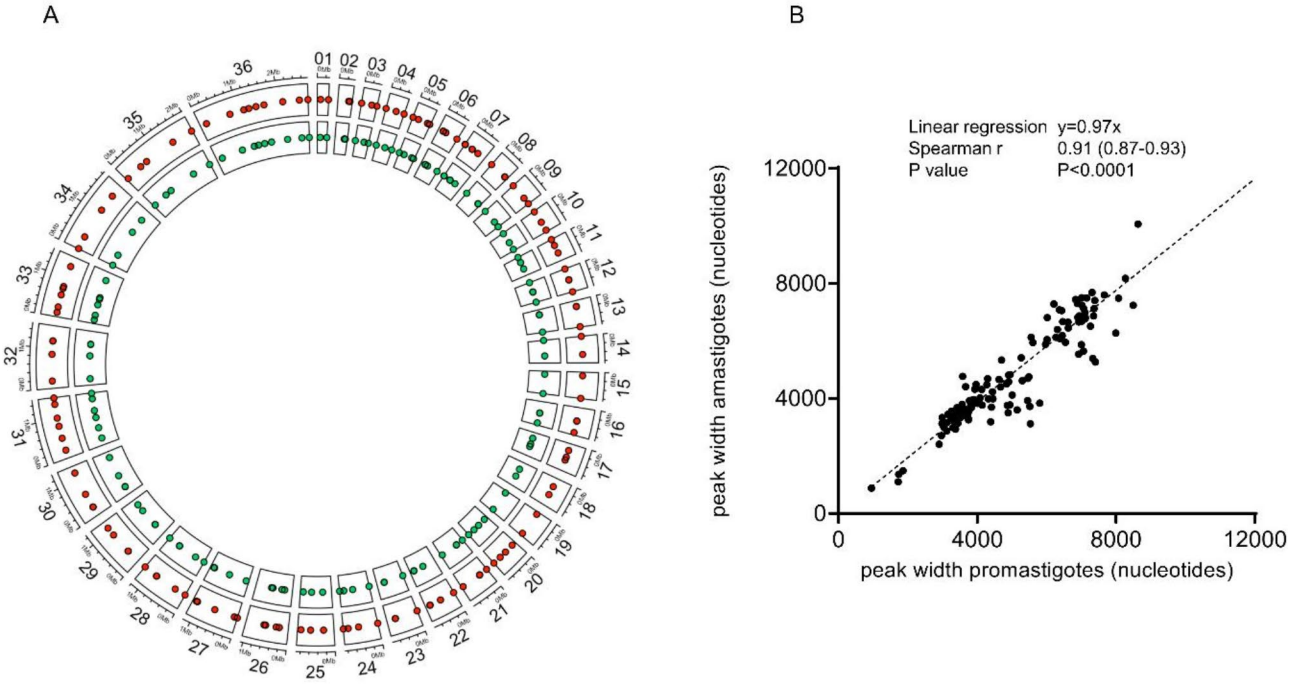

Fig. 5 Comparison of H3K4me3 enriched regions between *L. infantum* promastigotes and amastigotes. (**A**) Chromosome location of H3K4me3 enriched regions found in *L. infantum* promastigotes (red) and amastigotes (green). The circular plot has been done using circlize R package. (**B**) Scatter plot comparing H3K4me3 peak width values along the whole *L. infantum* genome between promastigotes and amastigotes. Spearman's correlation coefficients between the promastigotes and amastigotes and linear regression are shown in the graph. Two data points are outside the axis limit

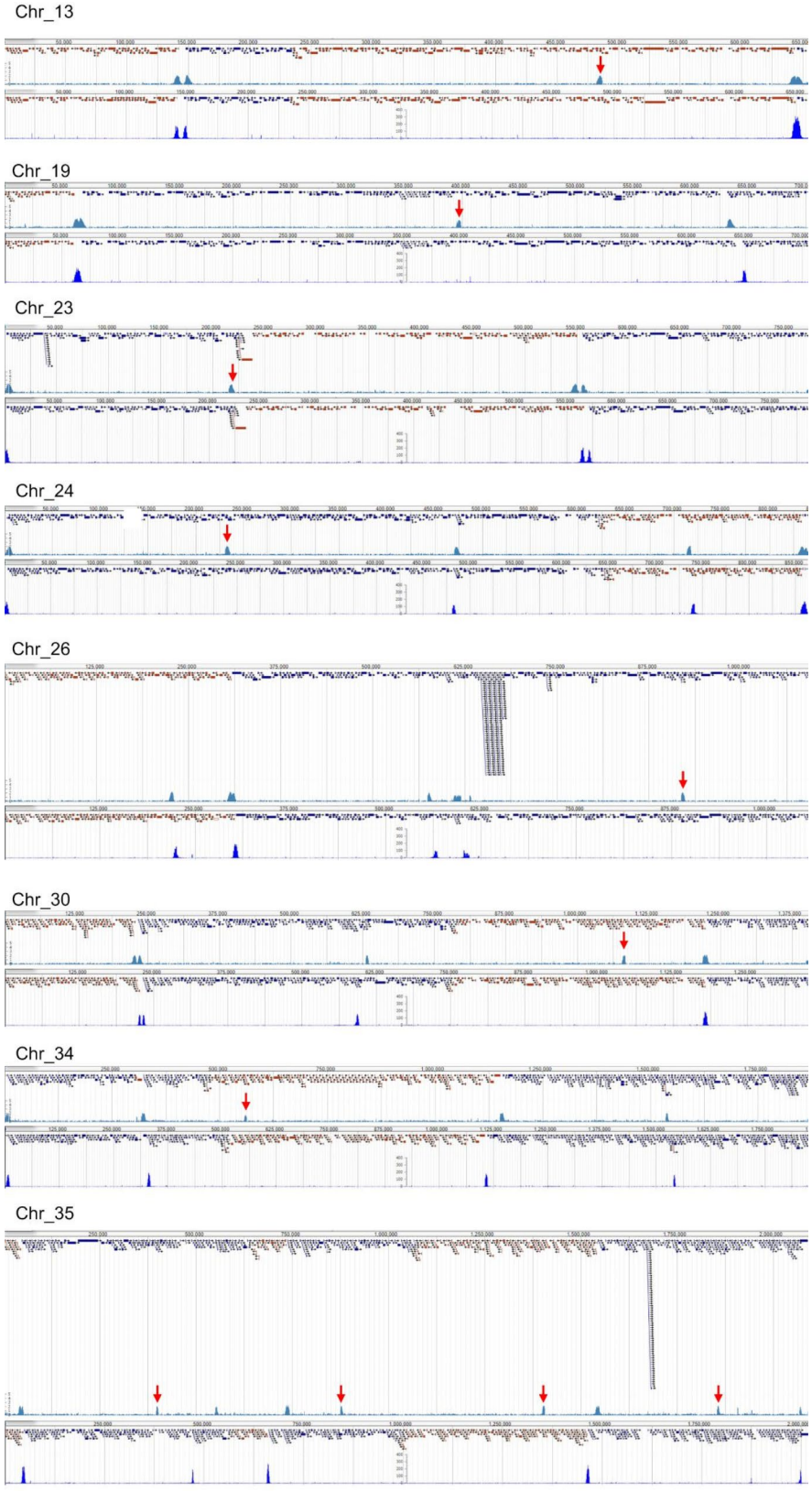

Fig. 6 Most of the H3K4me3 peaks in *L. infantum* co-localize with H3 acetylated peaks in *L. major*. Examples in chromosomes 13, 19, 23, 24, 26, 30, 34 and 35 of *L. major* (upper panels) and *L. infantum* (lower panels) are shown. Red arrows indicate *L. major* acetylated H3 peaks that do not have counterpart H3K4me3 peaks in the orthologous regions of *L. infantum*

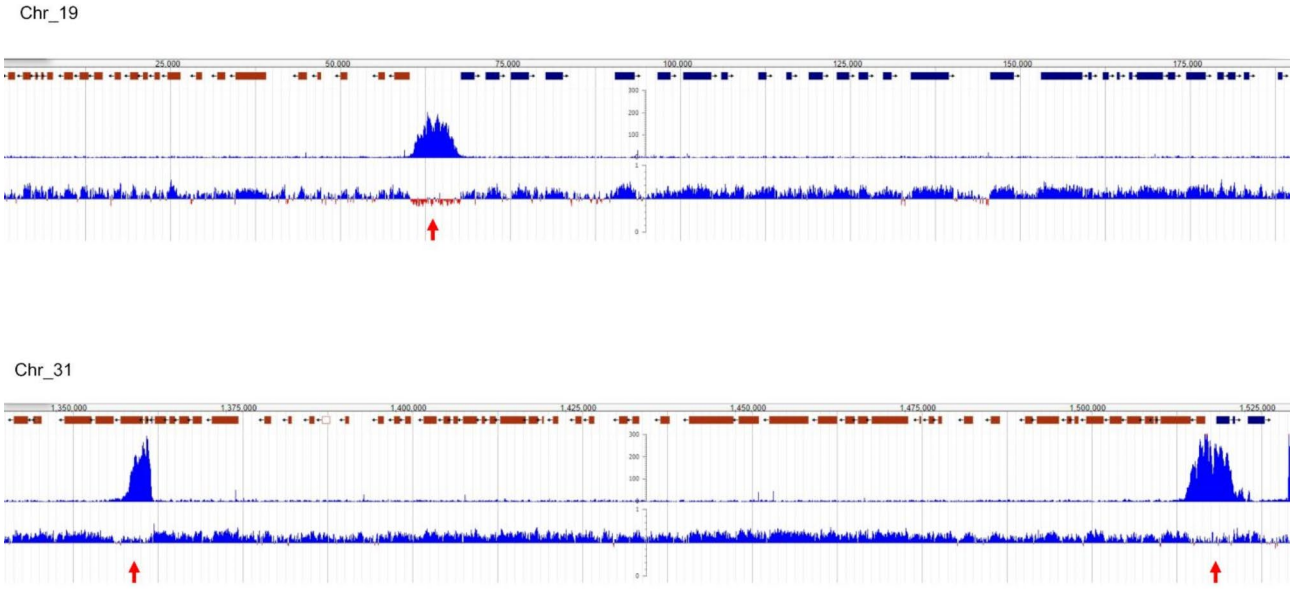

Fig. 7 H3K4me3 peaks along the *L. infantum* genome are associated with lower GC content. As an example, only portions of chromosomes 19 and 31 are shown. H3K4me3 enrichments and GC content are represented in upper and lower track, respectively. Red arrows indicate GC content in correspondence with H3K4me3 enrichments

width of those regions was around 5 kb, broader than the sharp, narrow peaks (< 1 kb) usually found in mammals at the 5' end of active genes [39]. To the best of our knowledge, this is the first time that H3K4me3 enriched region profiles were compared between extracellular promastigotes and amastigotes residing into macrophages, indicating the absence of differences in histone H3K4me3 distribution along the genome during the different phases of *Leishmania* life cycle. Recently, in *L. donovani* it has been demonstrated that TSS present as open euchromatin in fast-growing promastigotes but as less-accessible heterochromatin in the amastigote stage, indicating a possible epigenetic control of gene accessibility in this parasite [40]. Since H3K4me3 enriched regions appear constant between promastigotes and amastigotes, it appears unlikely that this modification is involved in chromatin remodeling in *L. infantum*.

In trypanosomatids, nucleosomes located near transcription initiation regions contain histone H3, H4 and variants H2A.Z and H2B.V. The histone H3 in such nucleosomes is tri-methylated at K4 and acetylated at K9/K14, while the histone H4 is acetylated at K10 [5, 41]. Most of the studies leading to these findings were conducted on *Trypanosoma* spp. Here, we compared ChIP-chip data obtained from *L. major* chromatin immunoprecipitated with anti-K9/K14 acetylated histone H3 [21] and ChIP-seq data obtained in this work. This was possible since genome comparison among the *Leishmania* species (including *L. infantum* and *L. major*) has shown a high degree of conservation in terms of both gene content and gene synteny [37]. Nearly all *L. infantum* H3K4me3 peaks co-localized with *L. major* H3 acetylated peaks, accounting for the similar nucleosome positions/organization along the genomes of these two species. The only exceptions included some acetylated H3 peaks located at the end or internally of a polycistronic transcription unit; therefore, we confirmed that histone H3 acetylation and K4me3 occur in the same nucleosomes located at the TSS.

Due to high degree of syntheny between *L. infantum* and *L. major*, the lack of H3 acetylated and/or tri-methylated peaks in the genome of these two species may reflect possible annotation problems. For example, in chromosome 15, acetylated H3 peaks in *L. major* colocalize with H3K4me3 peaks in *L. infantum*. However, gene annotations in *L. infantum* is different, presenting a divergent SSR (i.e. a TSS) at position 204,000 which is lacking in *L. major* and other species. Therefore, the absence of H3K4me3 peak could account for a possible annotation problem in *L. infantum* JPCM5 genome. The same could be for the single annotated gene at the telomeric region in chromosome 22, which lack H3K4me3 peak.

Conclusions

In conclusion, these findings expand our knowledge of the H3K4me3 distribution in *L. infantum* either in its motile form (promastigote) and in the context of intracellular infection (amastigote) allowing us to study the parasite epigenome considering also the crosstalk that is established between the pathogen and the host cell. This will hopefully contribute to elucidate how the

H3K4me3 distribution is controlled in amastigotes and promastigotes.

Supplementary Information

The online version contains supplementary material available at https://doi.org/10.1186/s12864-025-11350-1.

Supplementary Material 1

Supplementary Material 2

Supplementary Material 3

Supplementary Material 4

Supplementary Material 5

Supplementary Material 6

Supplementary Material 7

Supplementary Material 8 (Figure 2 containing unprocessed images)

Supplementary Material 9 (additional file 2 containing unprocessed images)

Supplementary Material legends

Acknowledgements
Not applicable.

Author contributions
A.D. and S.A: conception, acquisition, analysis of data, manuscript drafting. G.P.: analysis of data. E.S., G.B.: acquisition, analysis of data. M.G. and M.F.: conception, interpretation of data. L.G.: conception, interpretation of data, manuscript drafting. All authors reviewed and approved the manuscript.

Funding
This work was partially supported by the Department of Biomolecular Sciences of University of Urbino, and FANOATENEO. The funders had no role in study design, data collection and analysis, decision to publish, or preparation of the manuscript.

Data availability
Sequence data that support the findings of this study have been deposited in Sequence Read Archive (SRA) BioProject PRJNA1069007 (https://www.ncbi.nlm.nih.gov/bioproject/PRJNA1069007) with accession numbers SAMN39609176-SAMN39609180.

Declarations

Ethics approval and consent to participate
Not applicable.

Consent for publication
Not applicable.

Competing interests
The authors declare no competing interests.

Author details
[1]Department of Biomolecular Sciences, University of Urbino Carlo Bo, Via Arco d'Augusto 2, Fano (PU) 61029, Italy
[2]Department of Experimental Oncology, IRCCS, European Institute of Oncology, Milan, Italy
[3]Department of Biomedical Sciences, University of Padua, Padova, Italy

Received: 19 June 2024 / Accepted: 11 February 2025
Published online: 20 February 2025

References

1. Kaufer A, Ellis J, Stark D, Barratt J. The evolution of trypanosomatid taxonomy. Parasit Vectors. 2017;10:287.
2. Akhoundi M, Kuhls K, Cannet A, Votýpka J, Marty P, Delaunay P, et al. A historical overview of the classification, evolution, and dispersion of Leishmania Parasites and sandflies. PLoS Negl Trop Dis. 2016;10:e0004349.
3. Ceccarelli M, Galluzzi L, Diotallevi A, Andreoni F, Fowler H, Petersen C, et al. The use of kDNA minicircle subclass relative abundance to differentiate between Leishmania (L.) infantum and Leishmania (L.) amazonensis. Parasit Vectors. 2017;10:239.
4. Vanhamme L, Pays E. Control of Gene Expression in Trypanosomes. Vol. 59, Microbiological Reviews. 1995.
5. Martínez-Calvillo S, Vizuet-de-Rueda JC, Florencio-Martínez LE, Manning-Cela RG, Figueroa-Angulo EE. Gene expression in Trypanosomatid parasites. J Biomed Biotechnol. 2010;2010:1–15.
6. Martínez-Calvillo S, Yan S, Nguyen D, Fox M, Stuart K, Myler PJ. Transcription of Leishmania major Friedlin chromosome 1 initiates in both directions within a single region. Mol Cell. 2003.
7. Allis CD, Jenuwein T. The molecular hallmarks of epigenetic control. Nat Rev Genet. 2016;17:487–500.
8. Alsford S, Horn D. Trypanosomatid histones. Mol Microbiol. 2004;53:365–72.
9. Amatori S, Tavolaro S, Gambardella S, Fanelli M. The dark side of histones: genomic organization and role of oncohistones in cancer. Clin Epigenetics 2021 131. 2021;13:1–21.
10. Martínez-Calvillo S, Romero-Meza G, Vizuet-de-Rueda JC, Florencio-Martínez LE, Manning-Cela R, Nepomuceno-Mejía T. Epigenetic Regulation of Transcription in Trypanosomatid Protozoa. Curr Genomics. 2018;19:140.
11. Siegel TN, Hekstra DR, Kemp LE, Figueiredo LM, Lowell JE, Fenyo D, et al. Four histone variants mark the boundaries of polycistronic transcription units in Trypanosoma Brucei. Genes Dev. 2009;23:1063–76.
12. Maree JP, Patterton HG. The epigenome of Trypanosoma Brucei: a regulatory interface to an unconventional transcriptional machine. Biochim Biophys Acta. 2014;1839:743–50.
13. De Jesus TCL, Nunes VS, Lopes MDC, Martil DE, Iwai LK, Moretti NS, et al. Chromatin proteomics reveals variable histone modifications during the life cycle of Trypanosoma Cruzi. J Proteome Res. 2016;15:2039–51.
14. Picchi GFA, Zulkievicz V, Krieger MA, Zanchin NT, Goldenberg S, de Godoy LMF. Post-translational modifications of Trypanosoma Cruzi canonical and variant histones. J Proteome Res. 2017;16:1167–79.
15. Kraus AJ, Vanselow JT, Lamer S, Brink BG, Schlosser A, Siegel TN. Distinct roles for H4 and H2A.Z acetylation in RNA transcription in African trypanosomes. Nat Commun 2020 111. 2020;11:1–15.
16. Zhang N, Jiang N, Zhang K, Zheng L, Zhang D, Sang X, et al. Landscapes of protein posttranslational modifications of African Trypanosoma parasites. iScience. 2020;23:101074.
17. de Lima LP, Poubel SB, Yuan ZF, Rosón JN, Vitorino FN, de Holetz L. Improvements on the quantitative analysis of Trypanosoma Cruzi histone post translational modifications: study of changes in epigenetic marks through the parasite's metacyclogenesis and life cycle. J Proteom. 2020;225:103847.
18. Mandava V, Fernandez JP, Deng H, Janzen CJ, Hake SB, Cross GAM. Histone modifications in Trypanosoma Brucei. Mol Biochem Parasitol. 2007;156:41–50.
19. Gassen A, Brechtefeld D, Schandry N, Arteaga-Salas JM, Israel L, Imhof A, et al. DOT1A-dependent H3K76 methylation is required for replication regulation in Trypanosoma Brucei. Nucleic Acids Res. 2012;40:10302–11.
20. Fu H, Maunakea AK, Martin MM, Huang L, Zhang Y, Ryan M et al. Methylation of histone H3 on lysine 79 associates with a group of replication origins and helps limit DNA replication once per cell cycle. PLoS Genet. 2013;9.
21. Thomas S, Green A, Sturm NR, Campbell DA, Myler PJ. Histone acetylations mark origins of polycistronic transcription in Leishmania major. BMC Genomics. 2009;10:152.
22. Jha PK, Khan MI, Mishra A, Das P, Sinha KK. HAT2 mediates histone H4K4 acetylation and affects micrococcal nuclease sensitivity of chromatin in Leishmania donovani. PLoS ONE. 2017;12.
23. Kumar D, Rajanala K, Minocha N, Saha S. Histone H4 lysine 14 acetylation in Leishmania Donovani is mediated by the MYST-family protein HAT4. Microbiology. 2012;158:328–37.
24. Chandra U, Yadav A, Kumar D, Saha S. Cell cycle stage-specific transcriptional activation of cyclins mediated by HAT2-dependent H4K10 acetylation of promoters in Leishmania donovani. PLOS Pathog. 2017;13:e1006615.
25. McDonald JR, Jensen BC, Sur A, Wong ILK, Beverley SM, Myler PJ. Localization of epigenetic markers in Leishmania Chromatin. Pathogens. 2022;11:930.

26. Castelli G, Galante A, Verde V, Lo, Migliazzo A, Reale S, Lupo T, et al. Evaluation of two Modified Culture Media for Leishmania infantum cultivation versus different culture media. J Parasitol. 2014;100:228–30.
27. Galluzzi L, Diotallevi A, De Santi M, Ceccarelli M, Vitale F, Brandi G, et al. Leishmania Infantum induces mild unfolded protein response in infected macrophages. PLoS ONE. 2016;11:e0168339.
28. O'Neill LP, VerMilyea MD, Turner BM. Epigenetic characterization of the early embryo with a chromatin immunoprecipitation protocol applicable to small cell populations. Nat Genet. 2006;38:835–41.
29. Amatori S, Persico G, Paolicelli C, Hillje R, Sahnane N, Corini F, et al. Epigenomic profiling of archived FFPE tissues by enhanced PAT-ChIP (EPAT-ChIP) technology. Clin Epigenetics. 2018;10:1–15.
30. Amatori S, Ballarini M, Faversani A, Belloni E, Fusar F, Bosari S et al. PAT-ChIP coupled with laser microdissection allows the study of chromatin in selected cell populations from paraffin-embedded patient samples. Epigenetics Chromatin. 2014;7.
31. Amatori S, Persico G, Cantatore F, Rusin M, Formica M, Giorgi L et al. Small molecule-induced epigenomic reprogramming of APL blasts leading to antiviral-like response and c-MYC downregulation. Cancer Gene Ther. 2022.
32. Persico G, Casciaro F, Amatori S, Rusin M, Cantatore F, Perna A, et al. Histone H3 lysine 4 and 27 Trimethylation Landscape of Human Alzheimer's Disease. Cells. 2022;11:734.
33. Hillje R, Luzi L, Amatori S, Persico G, Casciaro F, Rusin M, et al. Time makes histone H3 modifications drift in mouse liver. Aging. 2022;14:4959–75.
34. Casciaro F, Persico G, Rusin M, Amatori S, Montgomery C, Rutkowsky J, et al. The histone H3 K4me3, K27me3, and K27ac genome-wide distributions are differently influenced by sex in brain cortexes and gastrocnemius of the Alzheimer's Disease PSAPP Mouse Model. Epigenomes. 2021;5:26.
35. Afgan E, Baker D, Batut B, Van Den Beek M, Bouvier D, Ech M, et al. The Galaxy platform for accessible, reproducible and collaborative biomedical analyses: 2018 update. Nucleic Acids Res. 2018;46:W537–44.
36. Garcia-Silva MR, Sollelis L, MacPherson CR, Stanojcic S, Kuk N, Crobu L, et al. Identification of the centromeres of Leishmania major: revealing the hidden pieces. EMBO Rep. 2017;18:1968–77.
37. González-De La Fuente S, Peiró-Pastor R, Rastrojo A, Moreno J, Carrasco-Ramiro F, Requena JM et al. Resequencing of the Leishmania infantum (strain JPCM5) genome and de novo assembly into 36 contigs. Sci Rep. 2017;7.
38. Dacher M, Tachiwana H, Horikoshi N, Kujirai T, Taguchi H, Kimura H, et al. Incorporation and influence of Leishmania histone H3 in chromatin. Nucleic Acids Res. 2019;47:11637–48.
39. Beacon TH, Delcuve GP, López C, Nardocci G, Kovalchuk I, van Wijnen AJ, et al. The dynamic broad epigenetic (H3K4me3, H3K27ac) domain as a mark of essential genes. Clin Epigenetics. 2021;13:138.
40. Grünebast J, Lorenzen S, Zummack J, Clos J. Life Cycle Stage-Specific Accessibility of Leishmania donovani Chromatin at Transcription Start Regions. Gilbert JA, editor. mSystems. 2021;6.
41. Respuela P, Ferella M, Rada-Iglesias A, Åslund L. Histone acetylation and methylation at sites initiating Divergent Polycistronic transcription in Trypanosoma Cruzi. J Biol Chem. 2008;283:15884–92.

Publisher's note

Springer Nature remains neutral with regard to jurisdictional claims in published maps and institutional affiliations.